

Regular and chaotic dynamics of a fountain in a stratified fluid

O. A. Druzhinin and Yu. I. Troitskaya

Citation: *Chaos* **22**, 023116 (2012); doi: 10.1063/1.4704814

View online: <http://dx.doi.org/10.1063/1.4704814>

View Table of Contents: <http://chaos.aip.org/resource/1/CHAOEH/v22/i2>

Published by the [American Institute of Physics](#).

Related Articles

Bifurcation phenomena in an impulsive model of non-basal testosterone regulation
Chaos **22**, 013121 (2012)

Resonance phenomena and long-term chaotic advection in volume-preserving systems
Chaos **22**, 013103 (2012)

Is the Smagorinsky coefficient sensitive to uncertainty in the form of the energy spectrum?
Phys. Fluids **23**, 125109 (2011)

Neutrally buoyant particle dynamics in fluid flows: Comparison of experiments with Lagrangian stochastic models
Phys. Fluids **23**, 093304 (2011)

Complete chaotic mixing in an electro-osmotic flow by destabilization of key periodic pathlines
Phys. Fluids **23**, 072002 (2011)

Additional information on Chaos

Journal Homepage: <http://chaos.aip.org/>

Journal Information: http://chaos.aip.org/about/about_the_journal

Top downloads: http://chaos.aip.org/features/most_downloaded

Information for Authors: <http://chaos.aip.org/authors>

ADVERTISEMENT



AIP Advances

Submit Now

**Explore AIP's new
open-access journal**

- **Article-level metrics
now available**
- **Join the conversation!
Rate & comment on articles**

Regular and chaotic dynamics of a fountain in a stratified fluid

O. A. Druzhinin and Yu. I. Troitskaya
Institute of Applied Physics RAS, N. Novgorod 603950, Russia

(Received 15 March 2011; accepted 3 April 2012; published online 20 April 2012)

In the present paper, we study by direct numerical simulation (DNS) and theoretical analysis, the dynamics of a fountain penetrating a pycnocline (a sharp density interface) in a density-stratified fluid. A circular, laminar jet flow of neutral buoyancy is considered, which propagates vertically upwards towards the pycnocline level, penetrates a distance into the layer of lighter fluid, and further stagnates and flows down under gravity around the up-flowing core thus creating a fountain. The DNS results show that if the Froude number (Fr) is small enough, the fountain top remains axisymmetric and steady. However, if Fr is increased, the fountain top becomes unsteady and oscillates in a circular flapping (CF) mode, whereby it retains its shape and moves periodically around the jet central axis. If Fr is increased further, the fountain top rises and collapses chaotically in a bobbing oscillation mode (or B-mode). The development of these two modes is accompanied by the generation of different patterns of internal waves (IW) in the pycnocline. The CF-mode generates spiral internal waves, whereas the B-mode generates IW packets with a complex spatial distribution. The dependence of the amplitude of the fountain-top oscillations on Fr is well described by a Landau-type two-mode-competition model. © 2012 American Institute of Physics. [<http://dx.doi.org/10.1063/1.4704814>]

Complex behavior of many physical systems with many degrees of freedom sometimes can be described by modeling its dynamics with the use of a normal modes approach. In this approach, the dynamics of a few instability modes, and their interaction and competition, is considered retaining only lowest (usually second) order nonlinear terms in the governing equations. Here, we perform DNS and use the normal-modes modeling to study the dynamics of a fountain created by a vertical jet penetrating a density interface in a two-layer density stratified fluid. We find that the dynamics of the fountain can be described by a simple nonlinear model where just two instability modes are taken into account.

I. INTRODUCTION

A fountain is formed when a jet of heavier fluid is injected upwards into a lighter fluid (or air) environment. Rising of the heavy-fluid jet is opposed by the buoyancy (gravity) force, so that the jet axial vertical velocity decreases with height and at a certain point turns to zero. The heavier fluid further moves downward around the up-flowing fountain core. The dynamics of fountains is of interest due to many applications in hydrodynamics and geophysics and has been studied in laboratory experiments and numerical simulations.¹⁻⁴ Recently, a phenomenon of self-sustained oscillations of fountain-like flows has become of special interest.³ These results show that at sufficiently large Froude and Reynolds numbers [$Fr = U/(g'D)^{1/2}$ and $Re = UD/\nu$ where U and D are the fountain axial velocity and diameter at injection, $g' = g\Delta\rho/\rho$ the buoyancy jump defined by the gravity acceleration g , density jump $\Delta\rho$ and background density ρ , and ν the fluid kinematic viscosity] the steady, axisymmetric fountain flow becomes unstable

and the fountain-top oscillations develop. First, a circular flapping mode develops where the fountain is no longer axisymmetric and its top circles around the jet central axis. As the Fr and Re numbers are increased further, a bobbing mode becomes dominant where the fountain chaotically rises and collapses.³ A similar effect occurs if a submerged vertical jet flow reaches a water surface. The results of the laboratory experiment⁵ show that a fountain, created at the water surface by a plane, submerged vertical jet flow, becomes unsteady at sufficiently high Froude numbers, so that the fountain top oscillates in the vicinity of the jet vertical axis and generates surface waves.

In a fluid with a stable density stratification a fountain-like flow can be created by a jet propagating vertically from the lower layers of heavier fluid upwards into the upper layers. In practice, such fountains can be created, e.g., by buoyant plumes of waste water outfalls in the ocean in the presence of a seasonal thermocline.^{6,7} Satellite observations⁷ and laboratory experiments⁸ show that such vertically rising jets are capable of effectively generating internal gravity waves (IW) in the pycnocline. A theoretical model of this phenomenon was developed in Ref. 8, where self-sustained oscillations of the flow in the region where the rising jet flow is trapped by the pycnocline are considered as a source of IW.

The objective of the present study is to perform direct numerical simulation and theoretical analysis of the dynamics of a fountain created in a stably stratified fluid by a vertical, round jet flow penetrating a pycnocline. Governing equations and numerical method are described in Sec. II. Numerical results are discussed in Sec. III. A two-mode-competition model is presented and its predictions are compared with the direct numerical simulation (DNS) results in Sec. IV, and final conclusions are made in Sec. V.

II. BASIC EQUATIONS AND NUMERICAL METHOD

In DNS, a vertically propagating jet flow is created by injecting a flux of fluid with neutral buoyancy and circular, Gaussian velocity profile at a lower boundary of the computational domain (Fig. 1). A stable stratification of the fluid density is considered where a pycnocline is located at some distance above the lower horizontal boundary plane. The jet propagates upwards, deflects the pycnocline and penetrates a distance into the upper layer of lighter fluid. At a certain height, the jet fluid stagnates under the action of the gravity force and flows down around the up-flowing core. Finally, the jet fluid spreads in the horizontal plane at the neutral buoyancy level.

The Navier-Stokes equations for the fluid velocity are written under the Boussinesq approximation in the dimensionless form

$$\partial_t U_i + U_j \partial_j U_i = -\partial_i P + \frac{1}{\text{Re}} \partial^2 U_i - \frac{\delta_{iz}}{\text{Fr}^2} \rho, \quad (2.1)$$

$$\partial_j U_j = 0. \quad (2.2)$$

The equation for the fluid density is written as

$$\partial_t \rho + U_j \partial_j \rho + U_z \frac{d\rho_{ref}}{dz} = \frac{1}{\text{Re Pr}} \partial^2 \rho \quad (2.3)$$

In Eqs. (2.1)–(2.3), U_i ($i = x, y, z$) is the fluid velocity, ρ the instantaneous deviation of the fluid density from the reference profile $\rho_{ref}(z)$, and δ_{ij} the Kronecker's symbol. The density reference profile is considered in the form

$$\rho_{ref}(z) = 1 + 0.5[1 - \tanh 2(z - z_0)], \quad (2.4)$$

where z_0 defines the pycnocline location. In Eq. (2.3), the density ρ is normalized by the density jump across the pycnocline, and the viscous diffusion effect on $\rho_{ref}(z)$ is neglected.

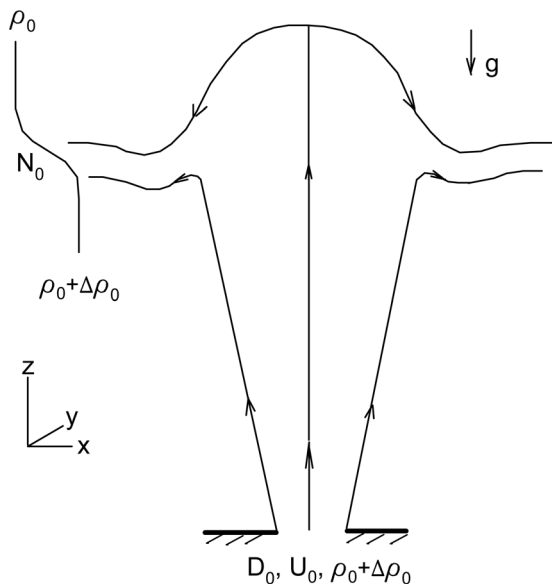


FIG. 1. Schematic of the flow.

Reynolds and Froude numbers are defined as

$$\text{Re} = \frac{U_0 D_0}{\nu}, \quad (2.5)$$

and

$$\text{Fr} = \frac{U_0}{N_0 D_0}, \quad (2.6)$$

where ν is the kinematic viscosity, U_0 and D_0 the velocity maximum and jet diameter at injection, and N_0 the buoyancy frequency in the middle of the pycnocline (at $z = z_0$). As follows from Eqs. (2.1)–(2.4), the corresponding dimensionless buoyancy frequency equals $N_m = 1/\text{Fr}$.

Equations (2.2)–(2.4) are discretized in a cubic domain with sizes $-15 \leq x \leq 15$, $-15 \leq y \leq 15$, and $0 \leq z \leq 30$ by employing a finite difference method of the second-order accuracy on a uniform rectangular staggered grid consisting of 200^3 nodes. The integration is advanced in time using the Adams-Bashforth method with time step $\Delta t = 0.015$. The Poisson equation for the pressure is solved by cosine transform [using fast Fourier transform (FFT)] over x and y coordinates, and Gauss elimination method over z coordinate.

The Neumann (zero normal gradient) boundary condition is prescribed for all fields in the horizontal (x) and spanwise (y) directions in the vertical side planes at $x = \pm 15$ and $y = \pm 15$, and at the upper horizontal plane in the vertical (z) direction, at $z = 30$. At the lower horizontal boundary plane, at $z = 0$, an injection condition for the velocity is prescribed in the form

$$U_i(x, y, z = 0, t) = \delta_{iz} \exp[-4(x^2 + y^2)], \quad (2.7)$$

where $i = x, y, z$. Here, the Neumann boundary condition for the pressure and density is also applied. Boundary conditions at injection used in the present paper are similar to the boundary conditions usually employed in DNS of spatially developing mixing layers (cf. Ref. 9 and references therein).

The pycnocline level z_0 in Eq. (2.4) is prescribed so that the jet interaction with the pycnocline is not affected by the boundaries of the computational domain and to be large enough ($z_0 = 20$ in dimensionless units) to allow the well-known self-similar structure of the jet flow propagating in a uniform environment to be established, and to minimize the effects of the fountain oscillations on the jet injection.

III. NUMERICAL RESULTS

DNS was performed for Froude numbers in the range $0 < \text{Fr} < 9$ with fixed Reynolds number $\text{Re} = 400$ and the boundary conditions discussed above. The Prandtl number was set equal to unity. At the initial time $t = 0$, the velocity and density fields, $U_i(x, y, z)$ and $\rho(x, y, z)$, were set equal to zero throughout the computational domain. Then, the injection condition (2.7) for the velocity was switched on “adiabatically,” i.e., proportionally to the factor $(1 - \exp(-t))$.

In order to check how the inflow boundary condition (2.7) complies with the demand of the mass conservation, we evaluated an instantaneous total fluid flux via the boundaries

of the computational domain ($F_S = \oint U_j n_j dS$, where n_j is the inner unit normal vector), and the volume integral of the divergence of the velocity field ($I_{div} = \int \partial_j U_j dV$). The results (not presented here) show that after a transient (for $t < 40$) the total velocity flux via boundaries as well as the volume integral of the velocity divergence becomes negligible. Thus, for later times, an initial transient a balance of the inflow via the lower horizontal boundary and the outflow via the vertical side boundaries is established.

All the transients died off and a statistically stationary distribution of the velocity and density fields was reached by the dimensionless time $t \approx 120$. From that time moment, the sampling of the velocity and density fields was performed to obtain time-averaged velocity and density fields and their respective rms fluctuations as well as frequency spectra of their oscillations. The sampling was performed during the time interval including 5 to 6 periods of internal waves generated in the pycnocline.

DNS results show that the flow remains axisymmetric and steady for sufficiently small Froude numbers. At some

critical, Froude number ($Fr > 2.5$), the flow becomes unstable. Depending on the Froude number, two different instability modes can be distinguished which are similar to the fountain oscillation modes observed in a homogeneous fluid: a circular flapping (CF) mode (for $3 < Fr < 5$) and a bobbing (B) mode ($Fr > 6$). If the circular flapping mode dominates, the top of the fountain retains its shape and moves in a horizontal plane around the jet vertical axis generating spiral internal waves in the pycnocline. If the bobbing mode becomes dominant (for larger Fr), the fountain top chaotically rises and collapses generating IW packets with relatively complex spatial distribution.

Figures 2–4 present the flow regimes observed in DNS for different Froude numbers: the steady fountain flow ($Fr = 2.5$, Fig. 2); the circular flapping mode ($Fr = 4$, Figs. 3(a) and 3(b)); and the bobbing mode ($Fr = 7$, Figs. 4(a) and 4(b)). The figures show the instantaneous distributions of the vorticity y -component ($\omega_y = \partial_z U_x - \partial_x U_z$) in the central vertical plane (x, z) and the density ρ in the horizontal plane (x, y) at the pycnocline level $z = z_0 = 20$.

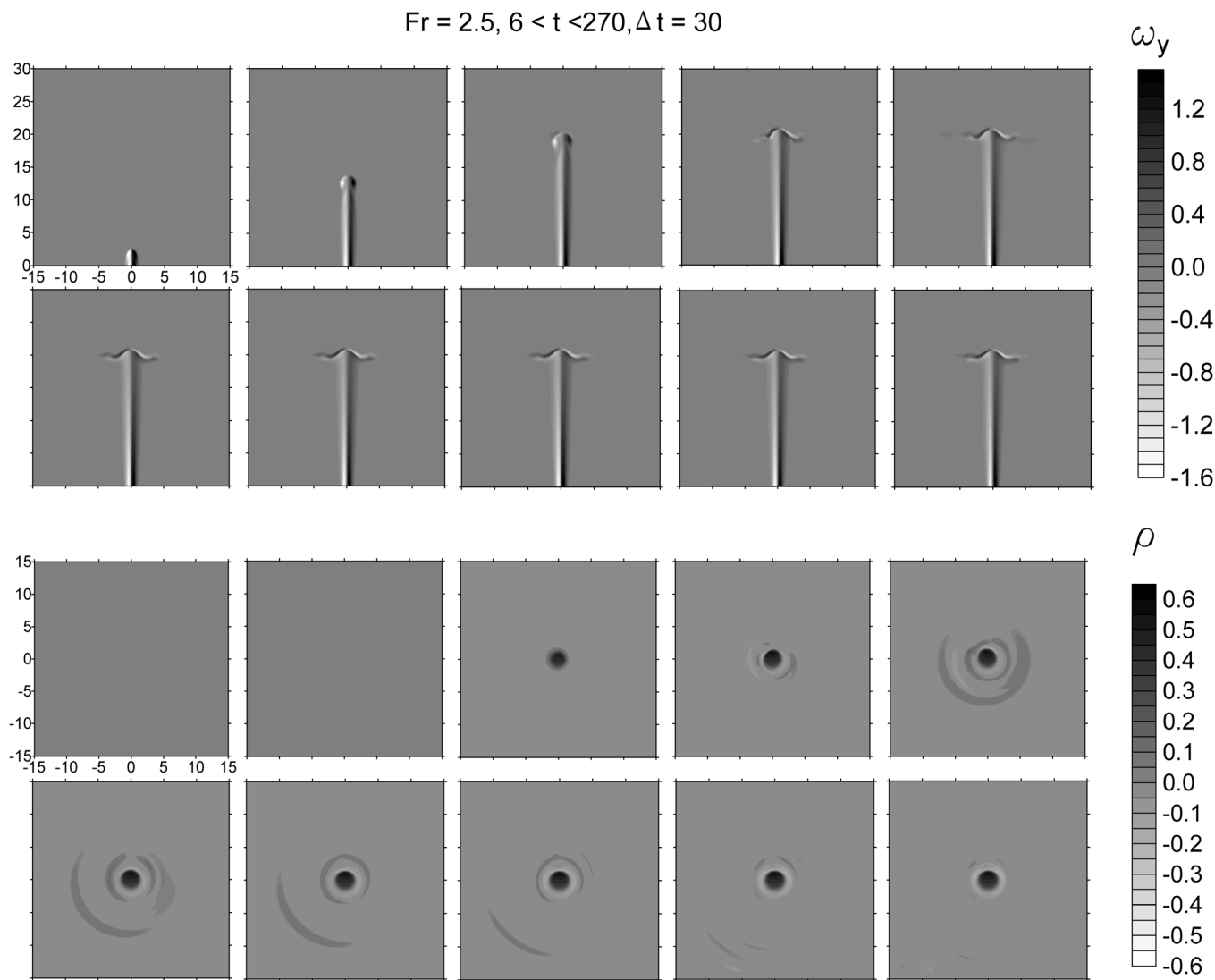


FIG. 2. Instantaneous distribution of the vorticity y -component ω_y in the central vertical plane (x, z) (top) and the density ρ in the horizontal plane (x, y) at the pycnocline level $z = 20$ (bottom) at obtained in DNS during the time interval $6 \leq t \leq 270$ for $Fr = 2.5$. The interval between the first two frames is $\Delta t = 24$ and the interval between the subsequent frames is $\Delta t = 30$.

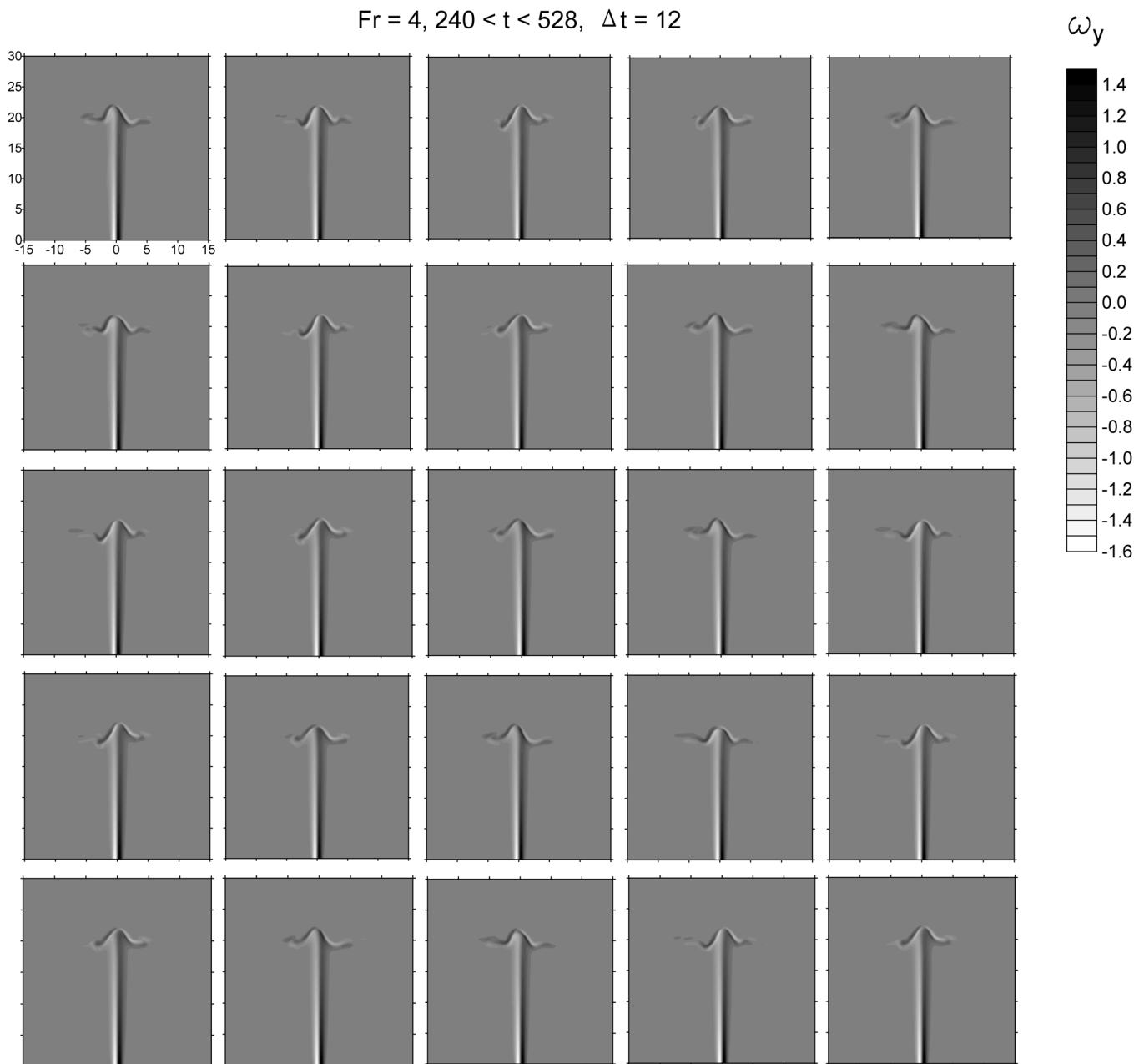


FIG. 3. (a) Instantaneous distribution of the vorticity y -component ω_y in the central vertical plane (x, z) obtained in DNS at different time moments for $Fr = 4$. The interval between the frames is $\Delta t = 12$ (b) instantaneous distribution of the density ρ in the horizontal plane (x, y) at the pycnocline level $z = 20$ at obtained in DNS at different time moments for $Fr = 4$.

Figure 2 shows that after a transient which occurs at times $t < 120$, an axisymmetric steady fountain flow is established. During the transient, the jet attains the pycnocline and distorts it. This interaction of the jet with the pycnocline is accompanied by the radiation of transient internal waves, which propagate radially toward the side boundaries and are subsequently damped due to the viscous diffusion effect. At later times, the flow remains steady and no internal waves are radiated by the fountain.

Figures 3 and 4 show the fountain top oscillations and IW generation which occur after the transient (at times $t > 240$) for Froude numbers $Fr = 4$ and $Fr = 7$, respectively. Figure 3 shows that in the case $Fr = 4$ the fountain oscillations occur in the CF-mode and are accompanied by the gen-

eration of internal waves having a spiral shape. In the case $Fr = 7$ (B-mode, Fig. 4), the fountain top rises and collapses chaotically and generates IW packets with complex spatial distribution propagating in the pycnocline from the center to the periphery of the computational domain.

Figs. 5(a) and 5(b) show the distributions of the horizontal and vertical components of the mean velocity, $\langle U_x \rangle$ and $\langle U_z \rangle$, mean density field $\langle \rho \rangle$, and rms fluctuation density field $\rho' = \langle (\rho - \langle \rho \rangle)^2 \rangle^{1/2}$ obtained in DNS for $Fr = 4$ (CF-mode) (a) and $Fr = 7$ (B-mode) (b). The figure shows that in both cases jet flow penetrates through the pycnocline a distance into the upper layer and stagnates at some height Z_m . Then, the jet fluid flows down around the up-flowing core and finally spreads in the horizontal plane

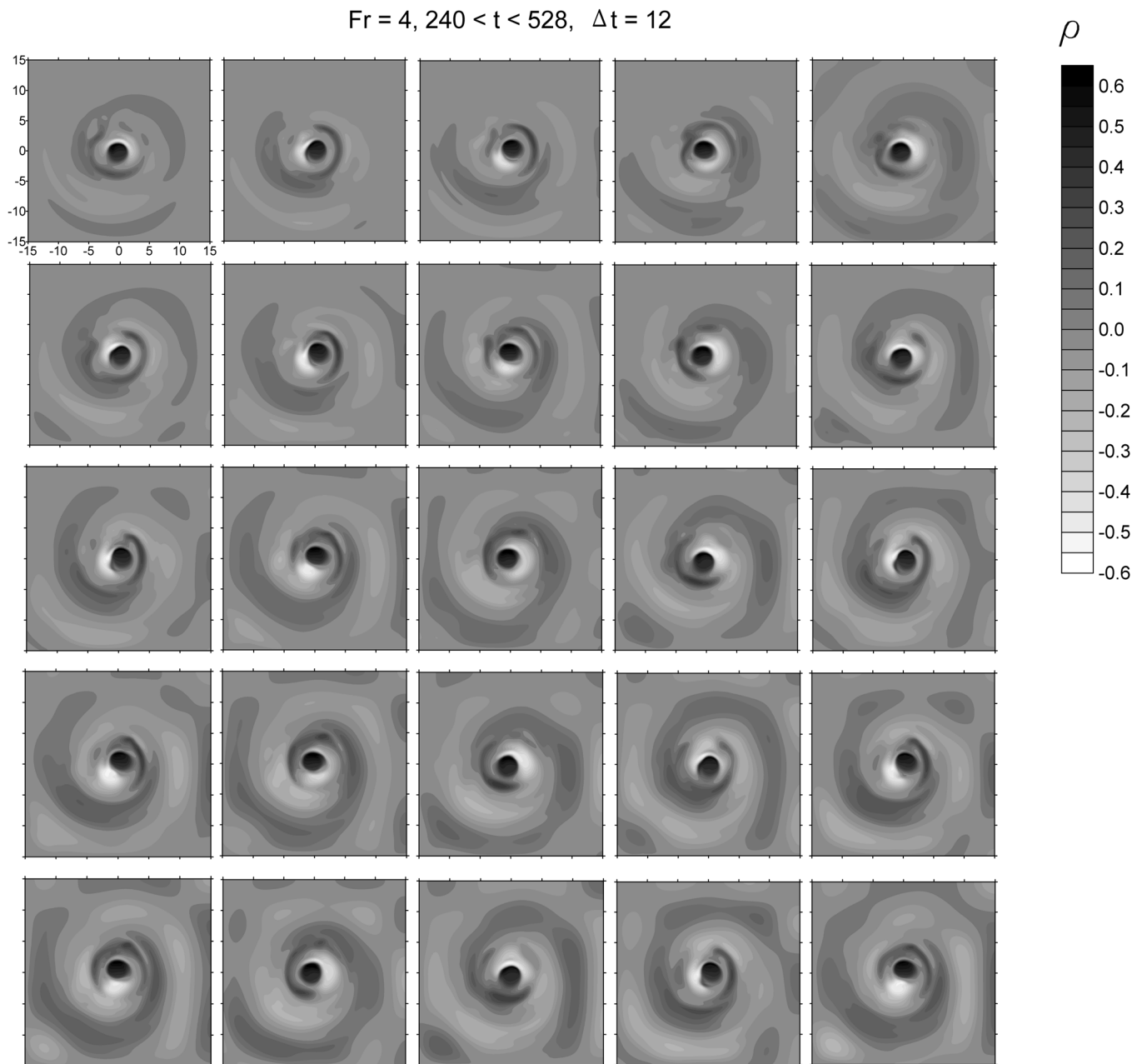


FIG. 3. (Continued).

in the vicinity of the pycnocline level at $z_0 = 20$ creating a radial outflow. Therefore, in the region $z_0 < z < Z_m$, a fountain is created.

Figure 5 shows that, as expected, the fountain height increases for larger Fr. The density fluctuation amplitude also increases with Fr. Moreover, in the case Fr = 4 (of CF-mode), the distribution of ρ' is characterized by maxima which occur at the flanks at some distance from the fountain central axis (at $x \approx \pm 1.5$), whereas for Fr = 7 (B-mode) ρ' has a maximum at the fountain center ($x = 0$). Figure 5(c) compares in detail the structure of the ρ' field in the vicinity of the fountain center for the two cases of Fr = 4 (i) and Fr = 7 (iii). This reflects a qualitative difference of the fountain dynamics distinguishing the two modes. The figure also shows the distribution of the ρ' field obtained from DNS with higher (300^3 -grid) resolution (to be discussed below).

At sufficiently large distance from the pycnocline level (in the region $0 < z < z_0$) the jet propagates in a uniform fluid environment. Since the amplitude of the fluctuations remains negligible in the considered region, the jet spatial development along the z -axis is governed by the viscous diffusion. Sufficiently far from injection (in the region $z \gg 1$), the jet flow development can be described by a self-similar solution in the form^{10,11}

$$U(x, y, z) = U_m(z) \exp\left(-4 \frac{x^2 + y^2}{D^2(z)}\right), \quad (3.1)$$

where the jet centerline velocity and diameter, U_m and D , are related as

$$U_m D = \text{const} \quad (3.2)$$

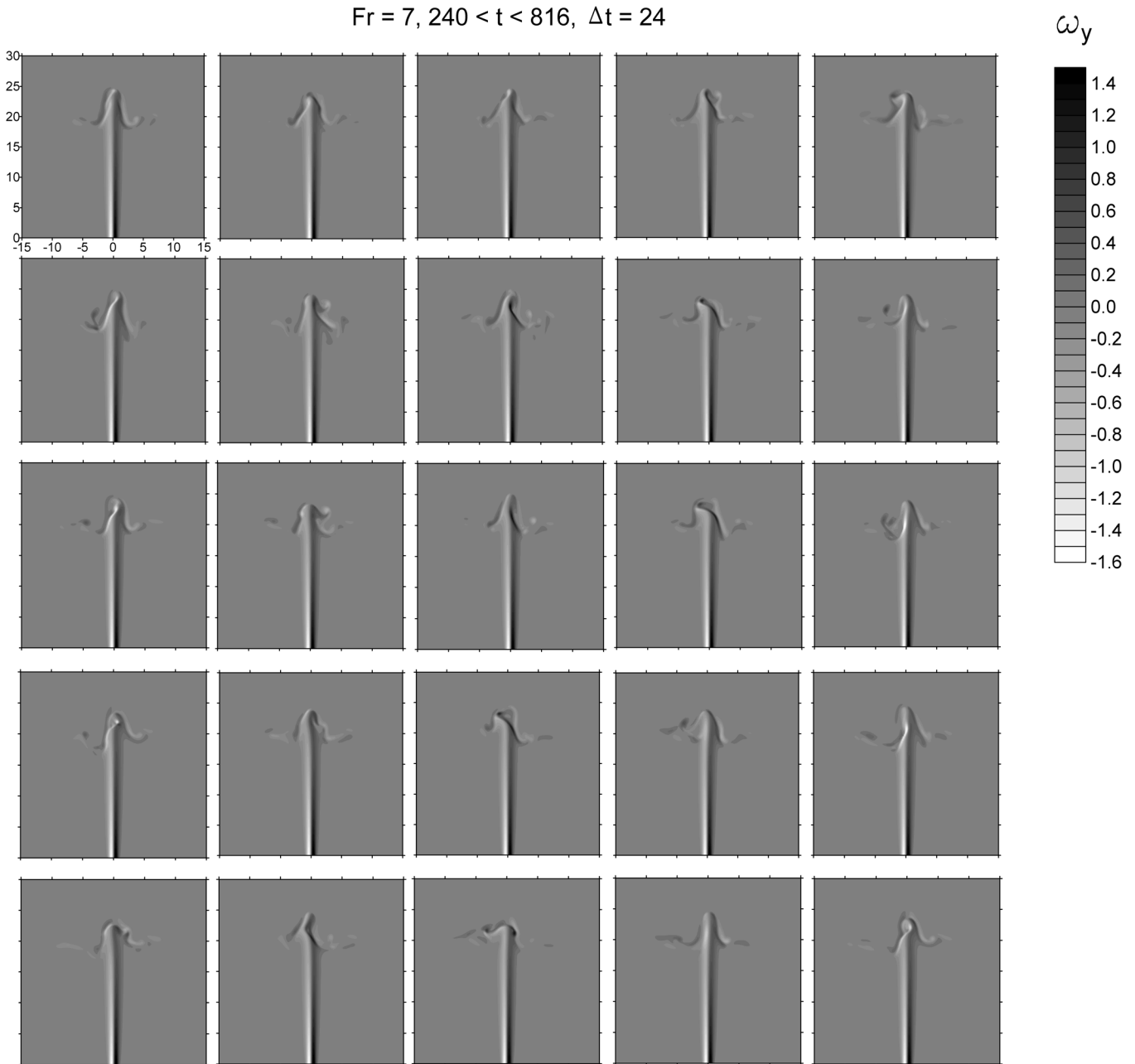


FIG. 4. (a) The same as in Fig. 3(a) but for $Fr = 7$. The interval between the frames is $\Delta t = 24$ and (b) the same as in Fig. 3(b) but for $Fr = 7$.

and asymptotically proportional to

$$U_m \sim z^{-1}, D \sim z \quad \text{for } z \gg 1. \quad (3.3)$$

From Eqs. (3.1)–(3.3), and (2.5), (2.6) follows that the jet Reynolds number remains constant, and the Froude number asymptotically decreases with height as

$$Fr \sim z^{-2} \quad \text{for } z \gg 1. \quad (3.4)$$

Figure 6 presents the profiles of the mean velocity $\langle U_z \rangle(x, 0, z)$ obtained in DNS for $Fr = 4$ and $Fr = 7$ at different heights and normalized by the centerline mean velocity $\langle U_z \rangle(0, 0, z)$ and the jet diameter defined from the mean velocity field (in Figs. 5(a) and 5(b)) as

$$D(z) = \frac{2 \int_{-L_x}^{L_x} \langle U_z \rangle(x, 0, z) dx}{\sqrt{\pi} \langle U_z \rangle(0, 0, z)}. \quad (3.5)$$

The figure shows that the profiles are well described by the self-similar solution (3.1). The figure also shows that the jet Reynolds number remains nearly constant in the region $4 < z < 15$ in agreement with Eq. (3.2). The figure also shows that the development of the jet centerline velocity $\langle U_z \rangle(0, 0, z)$ and Froude number is well predicted by fits

$$U_m = \frac{1}{0.05z + 1}, Fr(z) = \frac{Fr(0)}{(0.05z + 1)^2}, \quad (3.6)$$

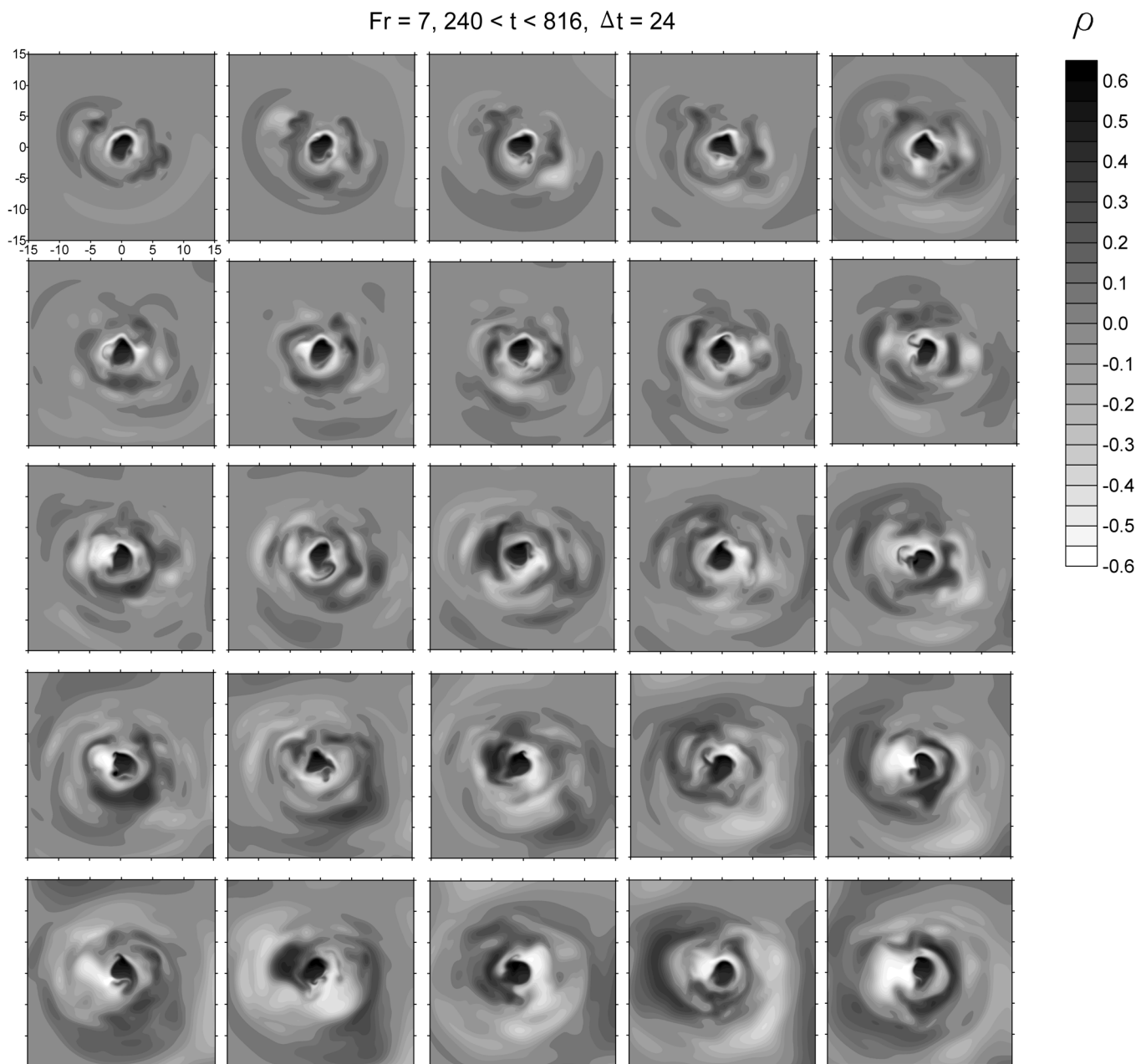


FIG. 4. (Continued).

which reproduce asymptotics (3.3), (3.4) for large z . At larger heights, the presence of the pycnocline significantly affects the jet vertical development, and the self-similarity of the jet is broken.

The difference between the CF-mode and the B-mode is also evident in the dynamics of the isopycnal surface ($Z_{\rho=1.5}(x, y) - z_0$), where the density is equal to the density in the middle of the unperturbed pycnocline, i.e., $\rho = \rho_{ref}(z_0) = 1.5$ (in dimensionless units), presented in Fig. 7. The figure shows that in the case of CF-mode (with $Fr = 4$) the fountain top circles around the central vertical axis at $(x = 0, y = 0)$ retaining its shape, whereas in the case of B-mode (with $Fr = 7$), the fountain top rises and collapses with no obvious periodicity.

Figure 8 presents spatially averaged frequency spectra of the oscillations of the isopycnal surface $Z_{\rho=1.5}$ and density

ρ obtained in DNS for $Fr = 4$ (CF-mode) and $Fr = 7$ (B-mode). Spectra of $Z_{\rho=1.5}$ were averaged over 10 realizations obtained at points equispaced in the range $-2 < x < 2$ at $y = 0$. The density (or IW) spectra were averaged over realizations obtained at 4 points located at $(x = \pm 10, y = 0)$ and $(x = 0, y = \pm 10)$ at the pycnocline level $z = z_0$. The figure shows that the spectra in the CF-mode case (for $Fr = 4$) are characterized by the well-defined maximum-amplitude peak with frequency $\omega/N \approx 0.5$ and its harmonics. On the other hand, in the B-mode case ($Fr = 7$), the spectra are continuous indicating that a chaotic regime sets in. In both cases, the location of the maximum-amplitude peak of IW spectra coincides with the location of that peak in the $Z_{\rho=1.5}$ spectra (at $\omega/N \approx 0.5$ for $Fr = 4$ and $\omega/N \approx 0.4$ for $Fr = 7$). The figure also shows the spectra obtained from DNS with higher (300^3 -grid) resolution (to be discussed below).

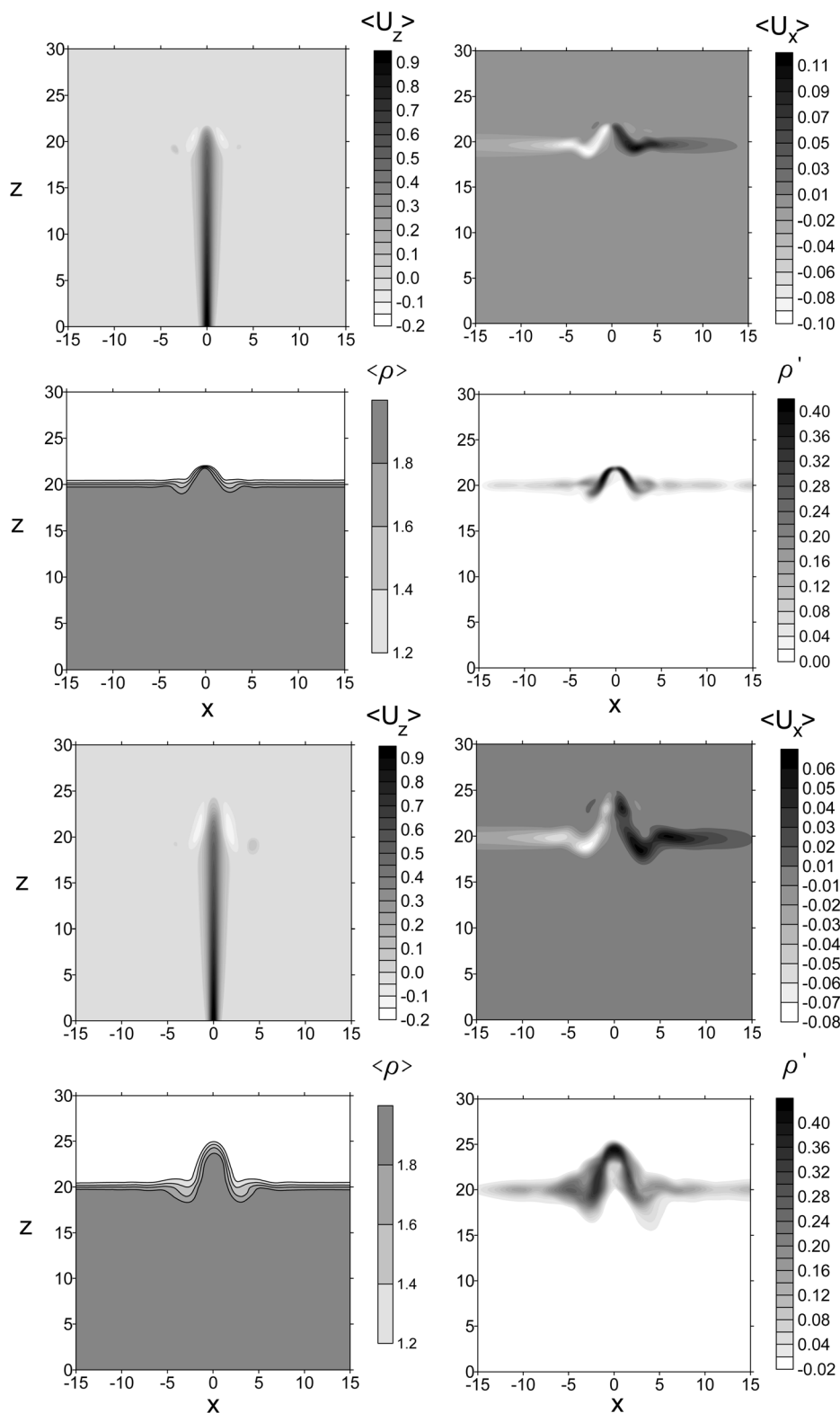


FIG. 5. (a) Distribution of the vertical and horizontal components of the mean velocity, $\langle U_z \rangle$ and $\langle U_x \rangle$, the mean density $\langle \rho \rangle$ and its rms fluctuation ρ' in the central vertical plane (x, z) obtained in DNS for Froude number $Fr = 4$ (b) the same as in Fig. 5(a) but for $Fr = 7$ (c) the details of the distribution of the density rms fluctuation ρ' in the central vertical plane (x, z) in the vicinity of the fountain center obtained in DNS for Froude number $Fr = 4$ (i) (CF-mode) and $Fr = 7$ (iii) (B-mode). Graphs in the right column (ii), (iv) are obtained from DNS with 300^3 -grid resolution. The contour levels are 0, 0.04, 0.08, ..., 0.44.

In order to find out how the flow characteristics depend on the Froude number DNS was performed $2.5 \leq Fr \leq 9$ with the same initial and boundary conditions. Figure 9 shows Fr -dependence of the fountain height, the dispersion

and frequency of the fountain-top oscillations, and the amplitude of internal waves.

Fountain height Z_m was evaluated as a maximum displacement of the isopycnal surface $Z_{\rho=1.5}(x, y = 0)$ with

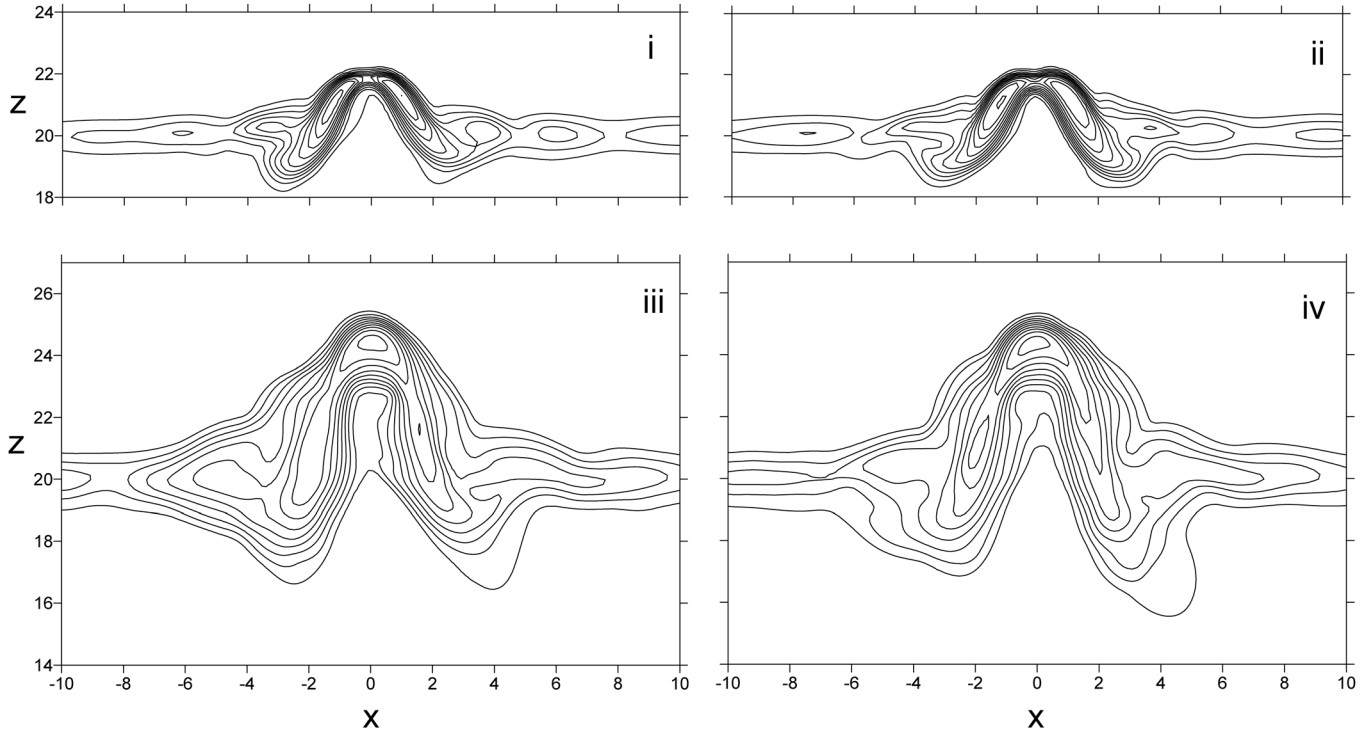


FIG. 5. (Continued).

respect to the initial pycnocline level z_0 and averaged over time. The dependence $Z_m(Fr)$ obtained in DNS is presented in Figure 9(a). Note that the height of a turbulent fountain is defined by the momentum and buoyancy fluxes in the dimensionless form as¹

$$Z_m^l \sim (U^2 D^2)^\alpha (UD^2 g \Delta \rho / \rho)^\beta D^{-1}, \quad (3.7)$$

with indexes $\alpha = 3/4$ and $\beta = -1/2$. As follows from Eq. (3.7),

$$Z_m^l \sim Fr. \quad (3.8)$$

On the other hand, the height of a laminar fountain is defined by the initial velocity and buoyancy jump across the pycnocline as

$$Z_m^l \sim U^2 / (Dg\Delta\rho/\rho) \sim Fr^2. \quad (3.9)$$

Figure 9(a) compares the dependence $Z_m(Fr)$ obtained in DNS with scaling $Z_m \sim Fr^{3/2}$ which can be regarded as an intermediate case of an unsteady fountain between the two limiting cases of fully turbulent and laminar fountains.² The figure shows that behavior of $Z_m(Fr)$ is in general agreement with this scaling.

Dispersion of the fountain-top oscillations Δ_Z was evaluated as an average dispersion of the oscillations of the isopycnal surface $Z_{\rho=1.5}(x, y = 0)$ obtained at 10 points equispaced in the range $-2 < x < 2$. Similarly, the IW amplitude ρ_{IW} was defined as an average dispersion of the density oscillations in 4 points located at $(x = \pm 10, y = 0)$ and $(x = 0, y = \pm 10)$ at the pycnocline level $z = z_0$. Figures 9(b) and 9(d) show that both Δ_Z and ρ_{IW} increase with

increasing Froude number for $Fr < 5$, under the regime of CF-mode oscillations. In the transient range $5 < Fr < 6$, Δ_Z and ρ_{IW} decrease, and further grow for $Fr > 6$ with increasing Froude number. The behavior of dispersion Δ_Z is well described by a stationary solution of the Landau's equation, which describes the growth of the amplitude of a disturbance under the regime of a small super-criticality¹⁰

$$\Delta_Z = \left(\frac{2\gamma}{\alpha} (Fr - Fr_c) \right)^{1/2}, \quad (3.10)$$

with parameters $\frac{2\gamma}{\alpha} = 0.4$ and $Fr_c = 3.6$ for $Fr < 5$, and $\frac{2\gamma}{\alpha} = 0.45$ and $Fr_c = 4.8$ for $Fr > 6$ (dashed lines in Fig. 9(b)). The fit for the numerical data in Fig. 9 for Δ_Z is sought in the form $C_1(Fr - C_2)^{1/2}$ where coefficients $C_{1,2}$ are varied to obtain better agreement separately for $3.5 < Fr < 5.5$ and $6 < Fr < 9$. The results in the figure indicate that the steady, axisymmetric fountain flow becomes unstable through the Andronov-Hopf bifurcation leading to the development of the fountain-top self-sustained oscillations. In the range $3 < Fr < 5$, the circular flapping mode is dominant, and the bobbing mode is dominant for $Fr > 6$. In Sec. IV, we discuss in more detail a two-modes-competition model and compare the model predictions with our DNS results.

Figure 9(c) shows that the frequency of the fountain-top oscillations (evaluated as a frequency of the maximum-amplitude peak in the spectrum of the oscillations of the isopycnal surface $Z_{\rho=1.5}$, cf. Fig. 8) which also coincides with the IW frequency, decreases monotonically as Fr increases. Note that the scaling for $\Omega_Z(Fr)$ can be derived under an assumption that the dimensionless frequency Ω_Z is defined by the relative buoyancy jump across the pycnocline,

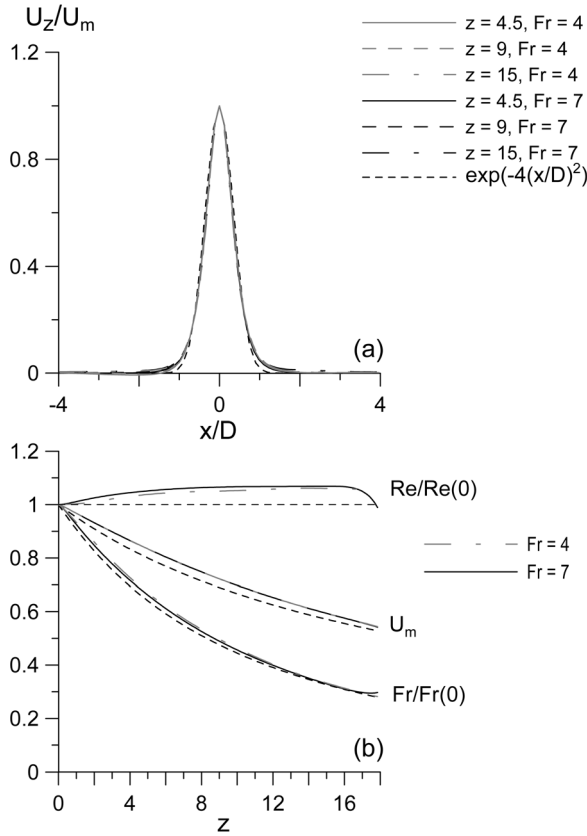


FIG. 6. Mean velocity profile $\langle U_z \rangle(x, y = 0)$ at different heights (a) and z -development of the jet centerline velocity U_m and the flow Reynolds and Froude numbers normalized by the respective initial values, Re ($z = 0$) and Fr ($z = 0$), for $Fr = 4$ and $Fr = 7$ (b) self-similar solution (3.1), (3.6) is shown in short-dashed line.

$g\Delta\rho/\rho$, and the flow length and velocity scales, D and U , so that

$$\Omega_Z \sim Dg\Delta\rho/\rho U^2 \sim Fr^{-2}. \quad (3.11)$$

This scaling is also observed experimentally for the fountain-top oscillations in the case of a heavy-fluid fountain in a surrounding homogeneous lighter fluid.³ (In this case, $\Delta\rho$ is the density difference between the fountain-fluid density and the surrounding fluid density.) Figure 9(c) shows that dependence $\Omega_Z(Fr)$ obtained in DNS is in general agreement with scaling (3.11) for $Fr > 5$.

In the above discussion, we characterize the dependence of the flow properties on Fr in terms of the Froude number at injection, i.e., $Fr = Fr(0)$. However, both Eq. (3.6) and Fig. 6 show that the Froude number decreases with height. Therefore, for practical purposes, it would be useful to characterize the Fr -dependence in terms of the Froude number in the vicinity of the pycnocline level, at $z \approx z_0$. On the other hand, Fig. 6 shows that the dependence of the Froude number vs. z -coordinate is the same for all $Fr(0)$ and well described by Eq. (3.6). Therefore, the characterization of the Fr -dependence of the flow dynamics in terms of $Fr(z_0)$ is reduced to the re-definition of the Froude number as $Fr(z_0) \approx 0.25 Fr(0)$. For convenience, we provide in Fig. 9 additional horizontal axes in terms of $Fr(z_0)$.

Figures 3–5 show that as IW propagates from the fountain center toward the side boundaries, their amplitude decreases (both due to the radial front expansion and the viscous diffusion effect). Thus, IW amplitude at the boundary decreases substantially as compared to the IW amplitude in the vicinity of the fountain center (from $\rho' \approx 0.1$ at $x \approx 5$ to $\rho' \approx 0.03$ at $x \approx 15$, cf. Figs. 5(a) and 5(b)). However, the waves reflected from the boundaries, although of a small amplitude, are still visible in Figs. 3(b) and 4(b). The reflected waves are also manifested in the distribution of the rms density fluctuations in Figs. 5(a) and 5(b) where local maxima of ρ' are present near boundaries $x = \pm 15$.

In order to find out how the fountain dynamics is affected by the internal waves reflected from the side boundaries we performed DNS for two Froude number cases, $Fr = 4$ and $Fr = 7$, in a larger domain with sizes $-30 \leq x \leq 30, -30 \leq y \leq 30$, and $0 \leq z \leq 30$ using the grid of $400 \times 400 \times 200$ nodes. Other DSN parameters and boundary conditions were the same as in the case of the cubic 30^3 -domain. The DNS results show that the distributions of the mean velocity and density in both cases are almost identical to these distributions obtained in the 30^3 -domain, and the spectra of the fountain-top oscillations and the IW spectra are also almost identical to the spectra from DNS with the 30^3 -domain. Therefore, the effect of the reflected waves on the fountain dynamics and the IW radiation by the fountain can be regarded as negligible.

In addition, we also performed a grid-dependence study to find out whether the observed fountain dynamics and the IW generation are properly resolved. In this study, we used the grid of $300 \times 300 \times 300$ nodes in the same 30^3 -domain and time step $\Delta t = 0.01$ and performed DNS for three characteristic cases of $Fr = 2.5$ (axisymmetric, steady fountain), $Fr = 4$ (CF-mode) and $Fr = 7$ (B-mode). The results show that the same scenario in the development of the fountain oscillations occurs as observed in DNS with 200^3 -grid (cf. Figs. 2–4). The spectra of the fountain-top oscillations and IW and the distribution of the rms density fluctuation in the central (x, z) -plane obtained in DNS with 200^3 -grid and 300^3 -grid are practically identical in all cases. Figure 5(c) shows that the structure of the CF and B modes of the fountain-top oscillations obtained from DNS with 300^3 -grid (ii) and (iv) are not changed. As in DNS with 200^3 -grid, for $Fr = 4$ (CF-mode), the distribution the maxima of ρ' occur at the flanks at some distance from the fountain central axis (at $x \approx \pm 1.5$), whereas for $Fr = 7$ (B-mode) ρ' has a maximum at the fountain center ($x = 0$). Thus, the qualitative difference of the fountain dynamics distinguishing the two modes is not changed. Figure 8 also shows that the location of the maximum-amplitude peaks in the spectra is not changed, and the difference between the peaks amplitudes is less than 4% in the case $Fr = 4$ and less than 1% in the case $Fr = 7$. Thus, we conclude that increasing the space and time resolution by 50% does not appreciably alter, both qualitatively and quantitatively, the observed fountain-top dynamics and IW generation, although considerably increases the required CPU-time and memory as compared to the DNS with 200^3 -grid.

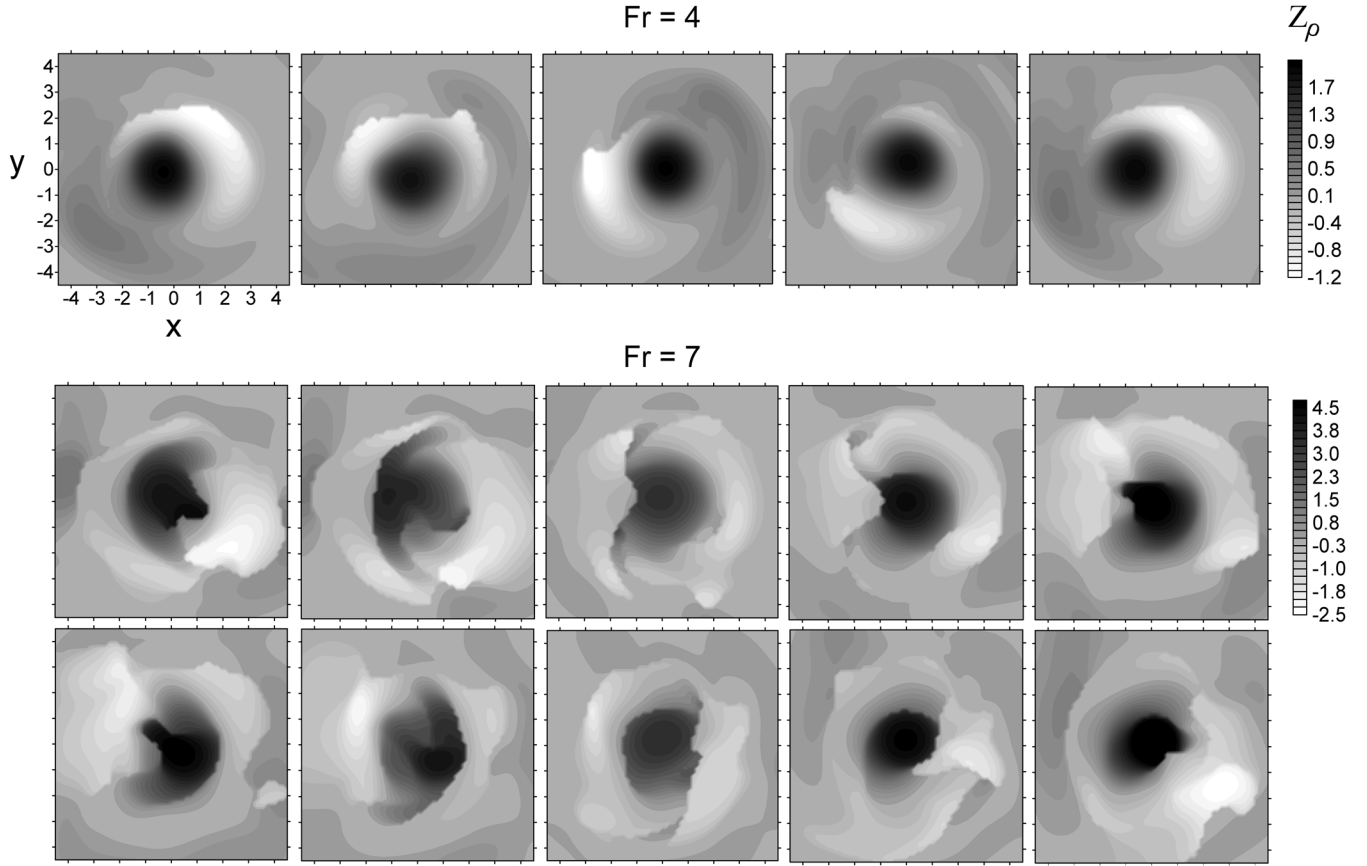


FIG. 7. Isopycnal surface ($Z_{\rho=1.5}(x, y) - z_0$) at time moments: $t = 342, 354, 366, 378, 390$ for $Fr = 4$, and $t = 420, 432, \dots, 728$ for $Fr = 7$.

IV. TWO-MODES-COMPETITION MODEL OF THE FOUNTAIN-TOP DYNAMICS

Let us employ the approach proposed by Landau for modeling the growth of a weak disturbance in a hydrody-

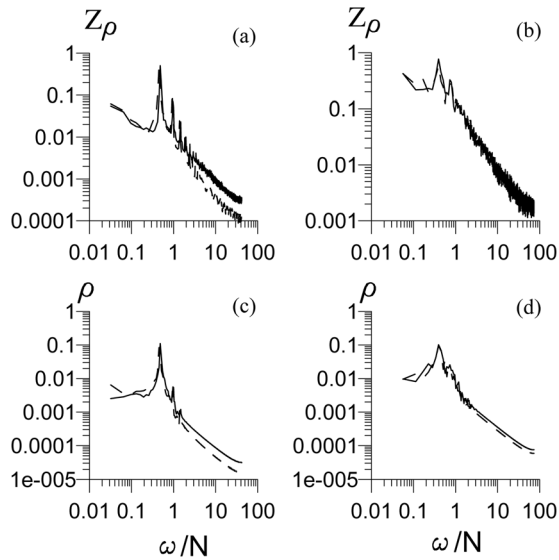


FIG. 8. Spatially averaged spectra of the oscillations of the isopycnal surface $Z_{\rho=1.5}$ in the region of the fountain-top and the density ρ at the pycnocline level $z = z_0$ at the distance of 10 dimensionless length units away from the fountain central axis for $Fr = 4$ (a), (c) (CF-mode) and $Fr = 7$ (b), (d) (B-mode). The buoyancy frequency $N = 1/Fr$. The spectra in dashed line are from DNS with higher (300^3 -grid) resolution.

namic system under the regime of a small super-criticality,¹⁰ and a phenomenological model of the development of self-sustained oscillations in a multi-frequency system.¹²

Consider a flow field consisting of a superposition of three parts, namely, the steady, axisymmetrical solution $U_0(x, y, z)$ and small-amplitude disturbances corresponding to two different modes

$$U_i(x, y, z, t) = A_0 U_{0i}(x, y, z) + \text{Re}\{A_1(t)U_{1i}(x, y, z) + A_2(t)U_{2i}(x, y, z)\}, \quad (4.1)$$

where $i = x, y, z$, $\text{Re}\{\}$ is the real part of the expression in the brackets, and the complex amplitudes of the first and second modes are written in the form

$$A_{1,2}(t) \equiv A_{1,2}(\beta_{1,2}t)\exp(-i\omega_{1,2}t). \quad (4.2)$$

In Eq. (4.2), $\omega_{1,2}$ are the real eigenfrequencies of the modes, and $\beta_{1,2}$ are the growth rates.

The system of equations for the modes amplitudes can be obtained by substitution of Eq. (4.1) into the original Navier-Stokes equations and linearization over small disturbances and time-averaging over oscillations with frequencies $\omega_{1,2}$.¹⁰ Consider the case of a small super-criticality where $\beta_{1,2}$ are linearly dependent on the governing parameter (the Froude number)

$$\beta_{1,2} = \gamma_{1,2}(Fr - Fr_{1,2}), \quad (4.3)$$

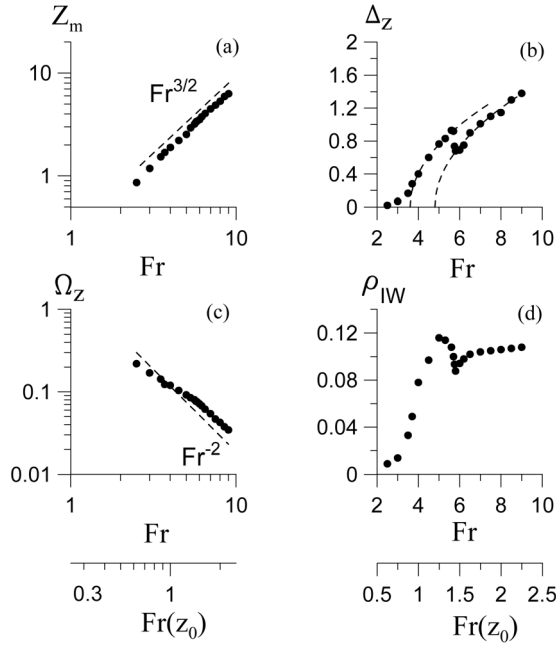


FIG. 9. Dependence of the fountain height Z_m (a), dispersion Δ_Z (b), and the maximum-peak frequency Ω_Z of the fountain-top oscillations (c), and IW amplitude ρ_{IW} (d) on Fr . Additional horizontal axes in terms of the Froude number at the pycnocline level, $Fr(z_0)$, are also provided.

where $\gamma_{1,2}$ are positive constants and $Fr_{1,2}$ the threshold values of the Froude number of the generation of the first and second modes, respectively. In accordance with the DNS results discussed in Sec. III, consider $Fr_1 < Fr_2$. In the case of a small super-criticality, the equations governing the temporal dynamics of the amplitudes can be written in the following normal form:^{10,12}

$$\frac{d|A_1|^2}{dt} = 2\gamma_1(Fr - Fr_1)|A_1|^2 - \alpha_1|A_1|^4 - r_1|A_1|^2|A_2|^2, \quad (4.4.1)$$

$$\frac{d|A_2|^2}{dt} = 2\gamma_2(Fr - Fr_2)|A_2|^2 - \alpha_2|A_2|^4 - r_2|A_1|^2|A_2|^2. \quad (4.4.2)$$

Second and third terms in the r.h.s. of Eq. (4.4) describe nonlinear interaction between the modes, and coefficients $\alpha_{1,2}$ and $r_{1,2}$ are assumed to be positive constants.^{10,12}

Consider the Froude number exceeding the threshold of the generation of the first mode, $Fr > Fr_1$. Then, it is convenient to introduce unknown positive functions $m_{1,2}$ related to the modes amplitudes as

$$|A_1|^2 = \frac{2\gamma_1}{\alpha_1}(Fr - Fr_1)m_1, \quad (4.5.1)$$

$$|A_2|^2 = \frac{2\gamma_2}{\alpha_2}(Fr - Fr_1)m_2, \quad (4.5.2)$$

and a “slow” time variable,

$$\tau = 2\gamma_1(Fr - Fr_1)t. \quad (4.5.3)$$

Substitution of Eqs. (4.5.1)–(4.5.3) into Eq. (4.4) gives the following equations for $m_{1,2}$:

$$\frac{dm_1}{d\tau} = m_1 - m_1^2 - R_1 m_1 m_2, \quad (4.6.1)$$

$$\frac{dm_2}{d\tau} = \mu m_2 - m_2^2 - R_2 m_1 m_2, \quad (4.6.2)$$

where $R_{1,2} = r_{1,2}/\alpha_{2,1}$ and

$$\mu = \frac{\gamma_2(Fr - Fr_2)}{\gamma_1(Fr - Fr_1)} \quad (4.7)$$

is the new governing parameter of the problem. From Eq. (4.7) follows that for $Fr > Fr_1$ parameter μ increases monotonically with increasing Fr , so that $-\infty < \mu \leq \gamma_2/\gamma_1$ for $Fr_1 \leq Fr < \infty$.

It can be shown by a straightforward calculation that Eq. (4.6) possess four steady solutions:

$$(m_1, m_2) = (0, 0), \quad (4.8.1)$$

$$(m_1, m_2) = (1, 0), \quad (4.8.2)$$

$$(m_1, m_2) = \left(\frac{1 - \mu R_1}{1 - R_1 R_2}, \frac{\mu - R_2}{1 - R_1 R_2} \right), \quad (4.8.3)$$

$$(m_1, m_2) = (0, \mu). \quad (4.8.4)$$

Solution (4.8.1) describes the steady axisymmetric flow and is unstable for $Fr > Fr_1$. Solutions (4.8.2) and (4.8.4) describe the generation of the first and second modes, respectively, and solution (4.8.3) describes a regime where the two modes coexist.

Linear stability analysis of solutions (4.8.1)–(4.8.4) shows that in the case $R_1 R_2 < 1$, or “weak” modes interaction, the following scenario develops as the Froude number increases. First, for $\mu < R_2$ only solution (4.8.2) is stable, so that the first (circular-flapping) mode is generated. As the Froude number increases, for $R_2 < \mu < 1/R_1$, solution (4.8.3) becomes stable and other solutions are unstable. Here, the two modes coexist, and the amplitude of the first (CF) mode decreases, whereas the amplitude of the second (bobbing) mode increases with Fr . As Fr is increased further, for $\mu > 1/R_1$, the only stable solution is Eq. (4.8.4) and describes the generation of the B-mode. The dependence of the modes amplitudes $|A_{1,2}|$ on Fr and the above scenario of the development of the interaction and competition between the modes are presented in Fig. 10(a) where $Fr_1^* = Fr(\mu = R_2)$, $Fr_2^* = Fr(\mu = 1/R_1)$ are the stability threshold values of the Froude number implicitly defined by Eq. (4.7).

In another case $R_1 R_2 > 1$, of “strong” interaction between the modes, the following scenario develops as the Froude number increases. For $\mu < 1/R_1$, the only stable solution is Eq. (4.8.2), so that CF-mode is generated. In the region $1/R_1 < \mu < R_2$ solutions (4.8.2) and (4.8.4) are both stable, so that either CF- or B-mode dominates the flow dynamics depending on initial conditions. The two-mode solution (4.8.3) in this case is unstable for all Fr . Fig. 10(b)

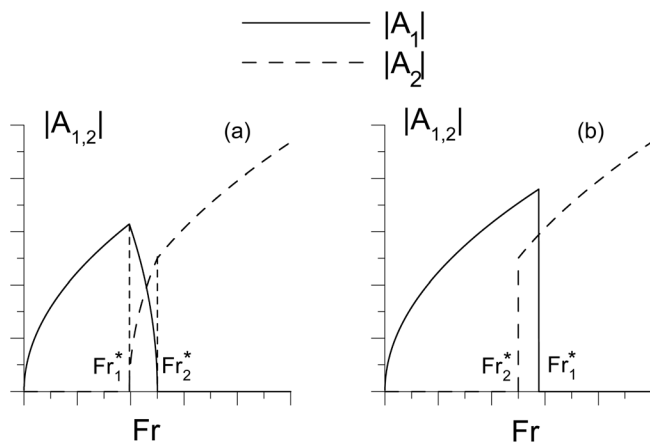


FIG. 10. Dependence of the modes amplitudes $|A_{1,2}|$ on the Froude number Fr in the cases of “weak” (a) and “strong” (b) interaction between the modes. $Fr_1^* = Fr(\mu = R_2)$, $Fr_2^* = Fr(\mu = 1/R_1)$.

shows dependence of the modes amplitudes on Fr in the considered case of “strong” mode interaction.

Figure 9(b) shows that the dependence of the dispersion of the fountain-top oscillations $\Delta_Z = (|A_1|^2 + |A_2|^2)^{1/2}$ on the Froude number experiences a jump at $Fr \approx 6$, where the regime of oscillations changes. Employing dependence $\Delta_Z(Fr)$ obtained in DNS the unknown coefficients in Eqs. (4.4)–(4.6) can be evaluated via a best-fit procedure as $\frac{2\gamma_1}{\alpha_1} \approx 0.41$, $\frac{2\gamma_2}{\alpha_2} \approx 0.45$, $R_1 \approx 2$, $R_2 \approx 0.47$, and the threshold values of the Froude number $Fr_1 \approx 3.6$ and $Fr_2 \approx 4.8$. Figure 11 shows that the theoretical approximation obtained within the weakly nonlinear asymptotical model fits well the DNS results. Therefore, the non-monotonous dependence $\Delta_Z(Fr)$ obtained in DNS can be regarded as the result of the competition between the CF- and B-modes.

It is important to point out that the model considered above does not take into account possible synchronization effects between the two modes which may affect their interaction. These synchronization effects are possible since the frequency of the fountain-top oscillations changes continuously in the range $5 < Fr < 6$ dividing the regimes dominated by the circular flapping and bobbing modes. However, the

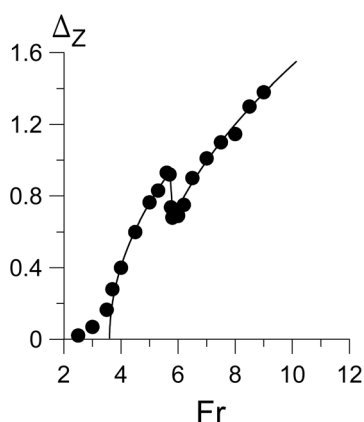


FIG. 11. Dependence of the dispersion of the fountain-top oscillations Δ_Z on Fr in DNS (symbols) and approximate solution of the two-modes-competition model $\Delta_Z = (|A_1|^2 + |A_2|^2)^{1/2}$ (in solid line).

agreement between the model prediction and DNS results in Fig. 11 indicates that the synchronization effects play a minor role in the considered case.

It should be also pointed out that in the general case, the model coefficients ($\gamma_{1,2}$, $\alpha_{1,2}$, and $r_{1,2}$) are also functions of the Reynolds number, i.e., dependent on the viscous diffusion effects. However, the experimental results and the regime map obtained in Ref. 3 show that for $Re > 300$ the behavior of the fountain is governed by the Froude number. Thus, $Re = 400$ considered in the present paper is large enough to neglect the viscous diffusion effects as far as the oscillations of the fountain top and generation of internal waves are concerned.

V. CONCLUSIONS

The dynamics of a fountain created by a vertical jet flow penetrating a pycnocline in a stably-stratified fluid has been studied by direct numerical simulation and theoretical analysis. The results show that if the flow Froude number Fr (defined by the initial velocity, diameter of the jet flow and the buoyancy frequency in the pycnocline) exceeds a threshold value ($Fr > 3$), the steady axisymmetric fountain flow becomes unstable and the fountain-top performs self-sustained oscillations accompanied by the generation of internal waves in the pycnocline. The results also show that there can be distinguished two different modes of the fountain-top oscillations. If the Froude number is small enough ($3 < Fr < 5$), the fountain-top moves periodically around the fountain central axis retaining its shape in a circular flapping mode and generates spiral internal waves (IW) in the pycnocline. If the Froude number is further increased, the fountain top collapses and rises chaotically in a bobbing oscillations mode and generates IW packets with a complex spatial distribution. The dependence of the amplitude of the fountain-top oscillations on Fr is well described by the Landau-type two-modes-competition model under the regime of small super-criticality.

ACKNOWLEDGMENTS

This work is supported by RFBR (11-05-00455, 11-08-97067, 12-05-01064).

¹J. S. Turner, “Jets and plumes with negative or reversing buoyancy,” *J. Fluid Mech.* **26**, 779–792, (1966).

²N. B. Kaye and G. R. Hunt, “Weak fountains,” *J. Fluid Mech.* **558**, 319–328 (2006).

³N. Williamson, N. Srinarayana, S. W. Armfield, G. D. McBain, and W. Lin, “Low-Reynolds-number fountain behavior,” *J. Fluid Mech.* **608**, 297–317 (2008).

⁴W. Lin and S. W. Armfield, “Direct simulation of weak axisymmetric fountains in a homogeneous fluid,” *J. Fluid Mech.* **403**, 67–68 (2000).

⁵V. P. Karlikov and O. V. Trushina, “On self-sustained oscillations of plane underwater fountains,” *Dokl. RAS.* **361**(3), 340–344 (1988) (in Russian).

⁶R. C. Y. Koh and H. N. Brooks, “Fluid Mechanics of waste-water disposal in the ocean,” *Ann. Rev. Fluid Mech.* **7**, 187–211 (1975).

⁷R. Keeler, V. Bondur, and C. Gibson, “Optical satellite imagery detection of internal wave effects from a submerged turbulent outfall in the stratified ocean,” *Geophys. Res. Lett.* **32**, L12610, doi:10.1029/2005GL022390 (2005).

⁸Yu. I. Troitskaya, D. A. Sergeev, E. V. Ezhova, I. A. Soustova, and V. I. Kazakov, "Auto-generation of internal waves by rising jets in a stratified tank," *Doclady RAS*. **419**(5), 691–695 (2008) (in Russian).

⁹O. A. Druzhinin and S. E. Elghobashi, "Direct numerical simulation of a three-dimensional spatially developing bubble-laden mixing layer with two-way coupling," *J. Fluid Mech.* **429**, 23–61 (2001).

¹⁰L.D. Landay and E. M. Livshitz, *Hydrodynamics* (Nauka, Moscow, 1988), 736p (in Russian).

¹¹G. N. Abramovich, *The Theory of Turbulent Jets* (Nauka, Moscow, 1984), 715p (in Russian).

¹²M. I. Rabinovich and D. I. Trubetskov, *Introduction into the Oscillations and Waves Theory* (Nauka, Moscow, 1984), 432p (in Russian).